

Adversarial Bipartite Graph Learning for Video Domain Adaptation

Yadan Luo¹, Zi Huang¹, Zijian Wang¹, Zheng Zhang^{2,3}, Mahsa Baktashmotlagh¹

¹The University of Queensland, ²Peng Cheng Laboratory, Shenzhen

³Bio-Computing Research Center, Harbin Institute of Technology, Shenzhen

lyadanluo@gmail.com, huang@itee.uq.edu.au, zijian.wang@uq.edu.au, darrenzz219@gmail.com, m.baktashmotlagh@uq.edu.au

ABSTRACT

Domain adaptation techniques, which focus on adapting models between distributionally different domains, are rarely explored in the video recognition area due to the significant spatial and temporal shifts across the source (i.e. training) and target (i.e. test) domains. As such, recent works on visual domain adaptation which leverage adversarial learning to unify the source and target video representations and strengthen the feature transferability are not highly effective on the videos. To overcome this limitation, in this paper, we learn a domain-agnostic video classifier instead of learning domain-invariant representations, and propose an Adversarial Bipartite Graph (ABG) learning framework which directly models the source-target interactions with a network topology of the bipartite graph. Specifically, the source and target frames are sampled as heterogeneous vertexes while the edges connecting two types of nodes measure the affinity among them. Through message-passing, each vertex aggregates the features from its heterogeneous neighbors, forcing the features coming from the same class to be mixed evenly. Explicitly exposing the video classifier to such cross-domain representations at the training and test stages makes our model less biased to the labeled source data, which in-turn results in achieving a better generalization on the target domain. The proposed framework is agnostic to the choices of frame aggregation, and therefore, four different aggregation functions are investigated for capturing appearance and temporal dynamics. To further enhance the model capacity and testify the robustness of the proposed architecture on difficult transfer tasks, we extend our model to work in a semi-supervised setting using an additional video-level bipartite graph. Extensive experiments conducted on four benchmark datasets evidence the effectiveness of the proposed approach over the state-of-the-art methods on the task of video recognition.

CCS CONCEPTS

• **Computing methodologies** → **Transfer learning**; *Activity recognition and understanding*.

KEYWORDS

Video Action Recognition; Domain Adaptation.

Permission to make digital or hard copies of all or part of this work for personal or classroom use is granted without fee provided that copies are not made or distributed for profit or commercial advantage and that copies bear this notice and the full citation on the first page. Copyrights for components of this work owned by others than ACM must be honored. Abstracting with credit is permitted. To copy otherwise, or republish, to post on servers or to redistribute to lists, requires prior specific permission and/or a fee. Request permissions from permissions@acm.org.

MM '20, October 12–16, 2020, Seattle, WA, USA

© 2020 Association for Computing Machinery.

ACM ISBN 978-1-4503-7988-5/20/10...\$15.00

<https://doi.org/10.1145/3394171.3413897>

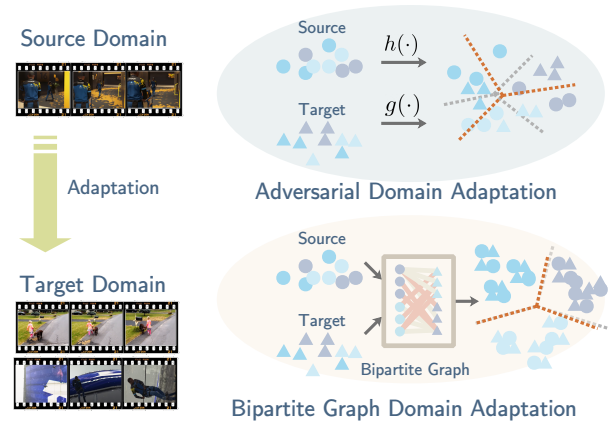


Figure 1: An illustration of the video domain adaptation task. With the unaligned inputs from different domains, the video classifier learned in existing adversarial DA approaches (shown as grey dotted lines) can easily overfit the labeled source data. By contrast, the classifier learned using our proposed ABG framework (shown as orange dotted lines) is domain-agnostic, which performs equally well at the training and test stages.

ACM Reference Format:

Yadan Luo¹, Zi Huang¹, Zijian Wang¹, Zheng Zhang^{2,3}, Mahsa Baktashmotlagh¹. 2020. Adversarial Bipartite Graph Learning for Video Domain Adaptation. In *Proceedings of the 28th ACM International Conference on Multimedia (MM '20)*, October 12–16, 2020, Seattle, WA, USA. ACM, New York, NY, USA, 9 pages. <https://doi.org/10.1145/3394171.3413897>

1 INTRODUCTION

With the advent of multimedia streaming [3, 23, 40, 41] and gaming data, automatically recognizing and understanding human actions and events in videos have become increasingly important, especially for practical tasks such as video retrieval [17], surveillance [28], and recommendation [42, 43]. Over the past decades, great efforts have been made to boost the recognition performance with deep learning for different purposes including appearances and short-term motions learning [33, 36], temporal structure modeling [39], and human skeleton and pose embedding [19, 31, 45]. While effective, deep learning enables machine recognition at a great cost of labeling large-scale data. To relieve the burden of tedious and expensive labeling, one alternative is to transfer knowledge from the existing annotated training data (i.e. **source domain**) to the unlabeled or partially labeled test data (i.e. **target domain**). However, the source

and target sets are commonly constructed under varying conditions such as illuminations, camera poses and backgrounds, leading to a huge domain shift. For instance, the Gameplay-Kinetics [2] dataset is built under the challenging “Synthetic-to-Real” protocol, where the training videos are synthesized by game engines and the test samples are collected from real scenes. In this case, the domain discrepancy between the source and target domains inevitably leads to a severe degradation of the model generalization performance.

To combat the above dilemmas, domain adaptation (DA) approaches have been investigated to mitigate the domain gap by aligning the distributions across the domains [1, 8, 46] or learning domain-invariant representations [6, 48]. While the notion of domain adaptation has been widely exploited in the past, the resulting techniques are mostly designed to cope with still images rather than the videos. These image-level DA methods could hardly achieve a good performance on the video recognition tasks as they don’t take into account the temporal dependency of the frames when minimizing the discrepancy between the domains.

Lately, video domain adaptation techniques [2, 11, 29] have emerged to address the domain shift in videos using adversarial learning. By segmenting the source and target videos into a set of fixed-length action clips, DAAA [11] directly matches the segment representations from different domains with the 3D-CNN [36] feature extractor. TA³N [2] weights the source and target segments with a proposed temporal attention mechanism, forcing the model to attend the temporal features of low domain discrepancy. Different from the prior work that mainly concentrates on intra-domain interactions, TcoN [29] proposes a cross-domain co-attention module to measure the affinity of the segment-pairs from source and target domains and further highlight the key segments shared by both domains.

Nevertheless, existing adversarial video domain adaptation methodologies are limited in three aspects. First, when data distributions embody complex structures like videos, there is no guarantee for the two distributions to become sufficiently similar when the discriminator is fully confused, as illustrated in Figure 1. Second, existing algorithms perform asymmetrically at the training and test stages. For instance, TcoN takes as input the source and target pairs and calculates the cross-domain attention scores at training stage, but inferences are done only based on the target data at the test time. This discrepancy unavoidably causes the exposure bias and deteriorates the model performance. Third, utilizing a general domain classifier for adversarial learning is only able to match marginal distributions [7], and so does not align the class-conditional distributions [20, 48]. The video recognition models trained in this manner are hereby less likely to achieve the class-wise alignment.

To address the above-mentioned issues, in this paper, we take a more feasible strategy, *i.e.*, to construct a domain-agnostic video classifier instead of pursuing with domain-invariant feature learning. In the proposed Adversarial Bipartite Graph (ABG) framework as illustrated in Figure 2, the video classifier is explicitly exposed to the mixed cross-domain representations, which preserves the temporal correlations across the domains modeled with a network topology of the bipartite graph. In particular, the source and target frames are sampled as heterogeneous vertexes of the bipartite graph, and the edges connecting the two types of nodes measure their similarity. Through message-passing, each vertex aggregates

the features of its heterogeneous neighbors, making those from the similar source and target frames to be evenly mixed in the shared subspace. The proposed strategy performs symmetrically during the training and test phases, which successfully addresses the exposure bias issue.

Moreover, as the proposed framework is agnostic to the choices of frame aggregation, four different aggregation mechanisms are investigated, followed by a conditional adversarial module to preserve the class-specific consistency across the domains. The source labels and the target predictions are embedded as vectors which provide semantic cues for the domain classifier. To cope with large domain discrepancy, we additionally apply a video-level bipartite graph on the original model, called Hierarchical ABG. To testify the robustness of the proposed model, we further extend it to a semi-supervised domain adaptation setting (Semi-ABG), by adding the partial edge supervision. Extensive experiments conducted on four benchmark datasets evidence the superiority of the proposed adversarial bipartite framework over the state-of-the-art approaches. Overall, our contributions can be briefly summarized as follows:

- We introduce a new Adversarial Bipartite Graph (ABG) framework for unsupervised video domain adaptation, which focuses on recognizing domain-agnostic concepts rather than learning domain-invariant representations. It is further generalized to its hierarchical variant for challenging transfer tasks.
- To address the exposure bias issue, the proposed model is trained and tested symmetrically.
- The proposed ABG framework is seamlessly equipped with a conditional domain adversarial module which globally aligns the class-conditional distributions from different domains.
- We have demonstrated the effectiveness of the proposed strategy through extensive experiments on four large-scale video domain adaptation datasets and released the source code for reference.

2 RELATED WORK

2.1 Video Action Recognition

Activity recognition has been one of the core topics in computer vision areas, with a wide range of real-world applications including video surveillance [28], environment monitoring and video captioning [5, 15, 38, 47]. A typical pipeline is leveraging a two-stream convolutional neural network to classify actions based on the individual video frames or local motion vectors [12, 33]. To better capture the action dynamics and gesture changes, later work models the long-term temporal information with recurrent neural networks [4], 3D convolutions [36], and multi-scale temporal relation networks (TRN) [49]. Another line of work augments the extracted RGB and optical flow features with multi-modal pose representations [45], complex object interactions [25], and 3D human skeleton [19, 31], which relieve the view dependency and the noises from different lighting conditions. However, the all above-mentioned work requires expensive annotations and could barely generalize to an unseen circumstance, which greatly hinders the feasibility in practice.

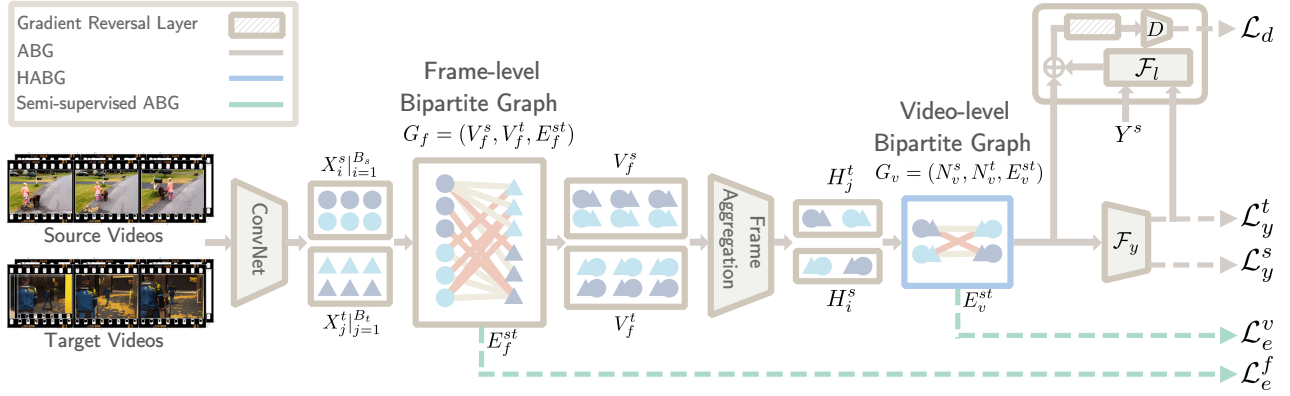


Figure 2: An overview of the proposed Adversarial Bipartite Graph (ABG) architecture, its hierarchical variant HABG (shown in blue), and the Semi-supervised ABG (shown in green).

2.2 Domain Adaptation

Unsupervised Domain Adaptation (UDA) tackles such a limitation by trying to transfer knowledge from a labeled source domain to an unlabeled target domain. The discrepancy between the two domains refers to the domain shift [22, 24], which is addressed by minimizing a distribution distance such as Maximum Mean Discrepancy (MMD) [8] with its variants [46] and/or learning domain-invariant representations with adversarial learning [6] recently. Alternatively, an emerging line of work incorporates graph neural networks (GNN) [9, 14, 37] to bridge the domain gap at a manifold level, learning the intra-domain correlations in a transductive way. Very recently, GCAN [26] constructs a densely-connected instance graph for the source and target nodes, and assigns pseudo labels for the target samples for aligning class centroids from different domains. While effective, existing graph-based work fails to model the inter-domain interactions, which makes it far from optimal.

2.3 Video Domain Adaptation

Despite of the fact that domain adaptation has made great progress in a broader set of image recognition tasks, it is barely investigated for transferring knowledge across the videos. Early efforts [35, 44] on video domain adaptation utilize a shallow model, that employs collective matrix factorization or PCA to learn a common latent semantic space for the source and target domains. Of late, the focus has shifted to the deep models [2, 11, 29]. Jamal *et al.* projected the pre-extracted C3D [36] representations of the source and target videos to a Grassmann manifold, and performed domain adaptation with adaptive kernels and adversarial learning. To extend the idea of modeling actions on the latent subspace, an end-to-end Deep Adversarial Action Adaptation (DAAA) [11] is derived to learn the source and target video clips in the same temporal order. Zhang *et al.* transferred from the trimmed video domain to the untrimmed video domain with Maximum Mean Discrepancy (MMD) [8] for action localization, yet without tasking into consideration any frame-level feature alignment. Chen *et al.* proposed a temporal attentive adversarial adaptation network (TA³N), which leverages the entropy of the domain predictor to attend the local temporal features of low domain discrepancy. Pan *et al.* [29] designed a co-attention

module to minimize the domain discrepancy, which concentrates on the key segments shared by the both domains. Nevertheless, prior work is vulnerable and unreliable due to the overfitting and exposure bias issues. Instead, the proposed adversarial bipartite graph model is capable of learning domain-agnostic concepts and aligning class-conditional distributions locally and globally.

3 METHODOLOGY

In this section, we first formulate the task of unsupervised video domain adaptation, and then elaborate the details of the derived Adversarial Bipartite Graph (ABG) framework and its hierarchical variant (HABG). To testify the robustness of the proposed model, it is further generalized to a semi-supervised setting (Semi-ABG) in Section 3.3.

3.1 Problem Formulation

Give a labeled source video collection $\mathcal{D}_s = \{(X_i^s, y_i)\}_{i=1}^{N_s}$ and an unlabeled target video set $\mathcal{D}_t = \{X_j^t\}_{j=1}^{N_t}$ containing N_s and N_t videos respectively, the aim is to design a transfer network for predicting the labels \mathcal{D}_t of the unlabeled target videos. The source and target domains are of different distributions yet they share the same label space $\mathcal{Y} \in \mathbb{R}^C$, where C is the number of classes. Each source video X_i^s or target video X_j^t consists of K frames, i.e., $X_i^s = \{x_i^k\}_{k=1}^K$ and $X_j^t = \{x_j^k\}_{k=1}^K$, where $x_i^k, x_j^k \in \mathbb{R}^D$ indicate the features of the k -th frame, and D is the feature dimension of the vectors. For constructing each mini-batch, we forward B_s source features and B_t target features to update the proposed model.

3.2 Adversarial Bipartite Graph Learning (ABG)

To model the data affinity across two domains, it is natural to formulate the problem with a bipartite graph, whose vertices can be divided into two disjoint and independent sets, with the edges connecting the vertices from different sets. As discussed in Section 3.2, the general pipeline of ABG consists of (1) mixing the similar source and target features with the frame bipartite graph; (2) aggregating frame features into the global video representations; (3) aligning class-conditional distributions with adversarial learning;

and (4) classifying the obtained source and target representations. To enhance the model capacity for difficult transfer tasks, we design a hierarchical structure HABG, incorporated in the video bipartite graph, as detailed in Section 3.2.

Frame-level Bipartite Graph. Let the frame-level directed bipartite graph be $G_f = (V_f^s, V_f^t, E_f^{st})$, where the cross-domain edge feature map $E_f^{st} \in \mathbb{R}^{K \cdot B_s \times K \cdot B_t}$ represents the node affinity between the pairs of source and target frames. The source vertex set $V_f^s = \{v_{ik}^s\}_{k=1}^K \in \mathbb{R}^{K \cdot B_s \times D_v}$ and target vertex set $V_f^t = \{v_{jk}^t\}_{k=1}^K \in \mathbb{R}^{K \cdot B_t \times D_v}$, with D_v the vertex feature dimension, are expected to dynamically aggregate information across the domains based on the learned edge features, thus closing the domain gap gradually. The propagation rules for the cross-domain edge update and node update are elaborated as follows.

Frame Edge Update. To calculate the similarity between the source and target frames, the normalized edge matrix is defined as,

$$\begin{aligned} A^f &= \sigma(\mathcal{F}_{fe}(|\mathcal{V}_f^s - \mathcal{V}_f^t|; \theta_{fe})), \\ \tilde{A}^f &= \frac{A_{i.}^f}{\|A_{i.}^f\|_1}, E_f^{st} = \frac{\tilde{A}_{.j}^f}{\|\tilde{A}_{.j}^f\|_1}, \end{aligned} \quad (1)$$

with σ the sigmoid function, and $\|\cdot\|_1$ the L_1 norm. $\mathcal{V}_f^s \in \mathbb{R}^{K \cdot B_s \times K \cdot B_t \times D_v}$ and $\mathcal{V}_f^t \in \mathbb{R}^{K \cdot B_s \times K \cdot B_t \times D_v}$ are the augmented tensors of the source and target vertexes, with the dimensions being expanded by repeating. $\mathcal{F}_{fe}(\cdot; \theta_{fe})$ is the frame-level metric network parameterized by θ_{fe} , which computes the similarity scores between the source and target frames. To ease the impact of the number of cross-domain neighbors, the row normalization and column normalization are adopted on the edge feature map E_f^{st} .

Frame Node Update. The generic rule to update node features can be formulated as follows,

$$\begin{aligned} \tilde{V}_f^s &= E_f^{st} V_f^t, \tilde{V}_f^t = (E_f^{st})^T V_f^s, \\ V_f^s &\leftarrow \mathcal{F}_{fv}([V_f^s; \tilde{V}_f^s]; \theta_{fv}), V_f^t \leftarrow \mathcal{F}_{fv}([V_f^t; \tilde{V}_f^t]; \theta_{fv}), \end{aligned} \quad (2)$$

where $[\cdot; \cdot]$ is the concatenation operation, and $\mathcal{F}_{fv}(\cdot; \theta_{fv})$ is a node update network for both source and target nodes. The node embedding is initialized with the extracted representation from the backbone embedding model, i.e., $V_f^s = \{(x_i^1, x_i^2, \dots, x_i^K)\}_{i=1}^{B_s} \in \mathbb{R}^{K \cdot B_s \times D}$, $V_f^t = \{(x_j^1, x_j^2, \dots, x_j^K)\}_{j=1}^{B_t} \in \mathbb{R}^{K \cdot B_t \times D}$.

Frame Aggregation. To group the sampled frames into a unified video representation and capture appearance and temporal dynamics, the frame aggregation is applied on the learned source and target node embeddings. As the proposed framework is agnostic to the choices of frame aggregation, we examine multiple aggregation functions, including a symmetric average pooling function which is invariant to the order of frames, two memory based modules to capture the temporal information among frames, and a temporal relation network to explore the multi-scale temporal dynamics.

Mean Average Pooling. By viewing the video as a collection of key frames, the video representation can be obtained by averaging the frame features temporally. Hence, each source video representation $H_i^s \in \mathbb{R}^{D_v}$ and target video representation $H_j^t \in \mathbb{R}^{D_v}$ are computed

as,

$$H_i^s = \frac{1}{K} \sum_{k=1}^K v_{ik}^s, H_j^t = \frac{1}{K} \sum_{k=1}^K v_{jk}^t. \quad (3)$$

Memory Based Aggregators. Considering the temporal characteristics in human actions and events, two memory based aggregators, i.e., LSTM and GRU, are tested to construct the i -th source representation $H_i^s = H_{iK}^s \in \mathbb{R}^{D_v}$, and j -th target representation $H_j^t = H_{jK}^t \in \mathbb{R}^{D_v}$ as:

$$\begin{aligned} H_{ik}^s &= \text{LSTM}(H_{ik-1}^s, v_{ik}^s), H_{jk}^t = \text{LSTM}(H_{jk-1}^t, v_{jk}^t), \\ H_{ik}^s &= \text{GRU}(H_{ik-1}^s, v_{ik}^s), H_{jk}^t = \text{GRU}(H_{jk-1}^t, v_{jk}^t), \end{aligned} \quad (4)$$

with H the output hidden states, and K the last step.

Temporal Relation Network (TRN). Inspired by [2, 49], we further build up on a fine-grained relationship among the multi-scale video segments. In particular, the temporal relation network (TRN) [49] is able to preserve the short-term (e.g., 2-frame relation), and long-term (e.g., 5-frame relation) action dynamics, which potentially expands the temporal information that the learned video features could convey. The multi-scale temporal relations for the source data $H^s \in \mathbb{R}^{B_s \times D_v}$ and the target data $H^t \in \mathbb{R}^{B_t \times D_v}$ are defined as the composite functions below,

$$\begin{aligned} T_2(V_f^s) &= \mathcal{G}\left(\sum_{k_1 < k_2} \mathcal{F}_t(v_{.k_1}^s, v_{.k_2}^s)\right), T_2(V_f^t) = \mathcal{G}\left(\sum_{k_1 < k_2} \mathcal{F}_t(v_{.k_1}^t, v_{.k_2}^t)\right), \\ H^s &= \sum_{k=2}^K T_k(V_f^s), H^t = \sum_{k=2}^K T_k(V_f^t), \end{aligned} \quad (5)$$

with the $T_2(\cdot)$ indicates the 2-frame local relation function. Note that the multi-scale function is the sum of the local relation scores from 2-frame to K -frame. The $\mathcal{F}_t(\cdot; \theta_t)$ and $\mathcal{G}(\cdot; \theta_G)$ are fully connected layers, fusing the features of different ordered frames.

Video-level Bipartite Graph. For difficult transfer tasks, we additionally apply a video-level bipartite graph on top of the frame aggregation network, fusing the source and target data hierarchically. It allows video features to be grouped into tighter clusters which improves classification performance. Similarly, we construct the video-level directed bipartite graph $G_v = (N_v^s, N_v^t, E_v^{st})$, where the $E_v^{st} \in \mathbb{R}^{B_s \times B_t}$ indicates the node affinity among the source and target videos. The source node set $N_v^s = \{n_i^s\}_{i=1}^{B_s} \in \mathbb{R}^{B_s \times D_n}$ and target node set $N_v^t = \{n_j^t\}_{j=1}^{B_t} \in \mathbb{R}^{B_t \times D_n}$, with D_n the feature dimension of video nodes, are learned through message passing as defined below.

Video Edge Update. To calculate the similarity between the source and target frames, the normalized edge matrix is defined as,

$$\begin{aligned} A^v &= \sigma(\mathcal{F}_{ve}(|\mathcal{N}_v^s - \mathcal{N}_v^t|; \theta_{ve})), \\ \tilde{A}^v &= \frac{A_{i.}^v}{\|A_{i.}^v\|_1}, E_v^{st} = \frac{\tilde{A}_{.j}^v}{\|\tilde{A}_{.j}^v\|_1}, \end{aligned} \quad (6)$$

with σ the sigmoid function, $\|\cdot\|_1$ the L_1 norm. $\mathcal{N}_v^s \in \mathbb{R}^{B_s \times B_t \times D_n}$ and $\mathcal{N}_v^t \in \mathbb{R}^{B_s \times B_t \times D_n}$ are the augmented tensors of the source and target vertices, with the dimensions being expanded by repeating.

$\mathcal{F}_{ve}(\cdot; \theta_{ve})$ is the video-level metric network parameterized by θ_{ve} , computing the correlations among the source-target video pairs.

Video Node Update. The generic rule to update the node features can be formulated as follows,

$$\begin{aligned} \tilde{N}_v^s &= E_v^{st} N_v^t, \quad \tilde{N}_v^t = (E_v^{st})^T N_v^s, \\ N_v^s &\leftarrow \mathcal{F}_{vn}([N_v^s; \tilde{N}_v^s]; \theta_{vn}), \quad N_v^t \leftarrow \mathcal{F}_{vn}([N_v^t; \tilde{N}_v^t]; \theta_{vn}), \end{aligned} \quad (7)$$

where $[\cdot; \cdot]$ is the concatenation operation and $\mathcal{F}_{vn}(\cdot; \theta_{vn})$ is a node update network for the both source and target nodes. The node embeddings are initialized with the aggregated features *i.e.*, $N_v^s = \{H_i^s\}_{i=1}^{B_s} \in \mathbb{R}^{B_s \times D_v}$, $N_v^t = \{H_j^t\}_{j=1}^{B_t} \in \mathbb{R}^{B_t \times D_v}$.

Video Classification. To predict the labels for the source and target samples, we construct a video classifier $\mathcal{F}_y(\cdot; \theta_y)$ based on the aggregated video features for the ABG structure and the video vertex features for the HABG, respectively. Since the source data is labeled, the classifier is trained to minimize the negative log likelihood loss for each mini-batch,

$$\mathcal{L}_y^s = -\frac{1}{B_s} \sum_{i=1}^{B_s} y_i \log(\mathcal{F}_y(n_i^s)). \quad (8)$$

Instead of the supervised loss, for the unlabeled target data, a soft entropy based loss is adopted to alleviate the uncertainty of the predictions:

$$\mathcal{L}_y^t = -\frac{1}{B_t} \sum_{j=1}^{B_t} \mathcal{F}_y(n_j^t) \log(\mathcal{F}_y(n_j^t)). \quad (9)$$

Conditional Adversarial Learning. Besides leveraging bipartite graph neural networks to fuse the source and target neighbors, a conditional adversarial module is applied to align the class-conditional distributions. To achieve this, the module is composed of a label embedding function $\mathcal{F}_l(\cdot; \theta_l)$ and a domain classifier $\mathcal{D}(\cdot; \theta_d)$. The label embedding function projects the i -th source video label y_i and the j -th target frame predictions $\mathcal{F}_y(n_j^t)$ into the latent vectors $\tilde{y}_i^s \in \mathbb{R}^{D_n}$ and $\tilde{y}_j^t \in \mathbb{R}^{D_n}$, providing the domain-invariant semantic cues for the domain classifier. The domain classifier is then conditioned on the classes for which the samples may belong to, and trained to discriminate between the features coming from the source or target data. The bipartite graphs are viewed as the feature generator to fool the discriminator. The adversarial objective function for the conditional adversarial module is formulated as:

$$\begin{aligned} \mathcal{L}_d &= \mathbb{E}_{n_i^s \sim N_v^s} \log[\mathcal{D}(n_i^s + \tilde{y}_i^s)] + \mathbb{E}_{n_j^t \sim N_v^t} \log[1 - \mathcal{D}(n_j^t + \tilde{y}_j^t)], \\ \tilde{y}_i^s &= \mathcal{F}_l(y_i; \theta_l), \quad \tilde{y}_j^t = \mathcal{F}_l(\mathcal{F}_y(n_j^t); \theta_l). \end{aligned} \quad (10)$$

Consequently, the learned features will be more discriminative and aligned when the two-player mini-max game reaches an equilibrium.

3.3 Semi-supervised ABG and HABG

To verify the robustness of the proposed ABG and HABG structure, we further extend them to a semi-supervised setting. In this circumstance, part of the target labels $y_\Omega^t \in \mathbb{R}^{|\Omega| \times C}$ in a mini-batch are available for training. Here, we denote Ω and $\neg\Omega$ as the indices of the labeled and unlabeled target data, respectively. To fully take advantage of the partial target supervision, the classification objective

functions are modified accordingly,

$$\begin{aligned} \mathcal{L}_y^s &= -\frac{1}{B_s} \sum_{i=1}^{B_s} y_i \log(\mathcal{F}_y(n_i^s)) - \frac{1}{|\Omega|} \sum_{j \in \Omega} y_j^t \log(\mathcal{F}_y(n_j^t)), \\ \mathcal{L}_y^t &= -\frac{1}{|\neg\Omega|} \sum_{j \in \neg\Omega} \mathcal{F}_y(n_j^t) \log(\mathcal{F}_y(n_j^t)), \end{aligned} \quad (11)$$

with $|\neg\Omega| = B_t - |\Omega|$. Moreover, the edge maps learned from either the frame-level or video-level bipartite graphs are able to be partially supervised. The newly added edge supervision is a binary cross entropy loss, which can be formulated as,

$$\begin{aligned} \mathcal{L}_e^f &= \sum_{i=1, j \in \Omega}^{B_s} \sum_{k=1}^K E_f^{st}(i+k, j+k) \delta(y_i = y_j^t), \\ \mathcal{L}_e^v &= \sum_{i=1, j \in \Omega}^{B_s} E_v^{st}(i, j) \delta(y_i = y_j^t), \end{aligned} \quad (12)$$

where $\delta(\cdot)$ is the Kronecker delta function that is equal to one when $y_i = y_j^t$, and zero otherwise. $E_f^{st}(i+k, j+k)$ indicates the element from the $(i+k)$ -th row and $(j+k)$ -th column of the frame-level edge map, and $E_v^{st}(i, j)$ represents the element from the i -th row and j -th column of the video-level edge map.

3.4 Optimization

Our ultimate goal is to learn the optimal parameters for the proposed model,

$$\begin{aligned} (\theta_{fe}^*, \theta_{fv}^*, \theta_a^*, \theta_{ve}^*, \theta_{vn}^*, \theta_l^*, \theta_y^*) &= \arg \min \mathcal{L} - \beta \mathcal{L}_d, \\ \theta_d^* &= \arg \min \mathcal{L} + \beta \mathcal{L}_d, \\ \mathcal{L} &= \mathcal{L}_y^s + \gamma \mathcal{L}_y^t + \lambda (\mathcal{L}_e^v + \alpha \mathcal{L}_e^f), \end{aligned} \quad (13)$$

with θ_a being the learnable parameters of the frame aggregation module, and β, γ, λ and α being the loss coefficients respectively. Notably, for the UDA setting, we have, $\mathcal{L}_e^f = 0$, and $\mathcal{L}_e^v = 0$. The overall algorithm is provided in supplementary material.

4 EXPERIMENTS

4.1 Datasets

We compare and contrast our proposed approach with the existing domain adaptation approaches on four benchmark datasets, *i.e.*, the **UCF-HMDB_{small}**, **UCF-HMDB_{full}**, **UCF-Olympic** and **Kinetics-Gameplay**. For fair comparison, we follow the dataset partition and feature extraction strategies from [2], that utilizes the ResNet101 model pre-trained on ImageNet as the frame-level feature extractor. The statistics of the four datasets are summarized in Table 1. The **UCF-HMDB_{small}** and **UCF-HMDB_{full}** are the overlapped subsets of two large-scale action recognition datasets, *i.e.*, the UCF101 [34] and HMDB51 [16], covering 5 and 12 highly relevant categories respectively. The **UCF-Olympic** selects the shared 6 classes from the UCF101 and Olympic Sports Datasets [27], including *Basketball, Clearn and Jerk, Diving, Pole Vault, Tennis and Discus Throw*. The **Kinetics-Gameplay** is the most challenging cross-domain dataset, with a large domain gap between the synthetic videos and real-world videos. The dataset is build by selecting 30 shared categories between Gameplay [2] and one of the largest

Table 1: The general statistics of the four datasets used in our experiments.

Property	UCF-HMDB _{small}	UCF-HMDB _{full}	UCF-Olympic	Kinetics-Gameplay
Video Length	~21 Seconds	~33 Seconds	~39 Seconds	~ 10 Seconds
Classes	5	12	6	30
Training Videos	UCF: 482 / HMDB: 350	UCF:1,438 / HMDB: 840	UCF: 601 / Olympic: 250	Kinetics: 43,378 / Gameplay: 2,625
Validation Videos	UCF: 189 / HMDB: 571	UCF: 360 / HMDB: 350	UCF: 240 / Olympic: 54	Kinetics: 3,246 / Gameplay: 749

public video datasets Kinetics-600 [13]. Each category may also correspond to multiple categories in both dataset, which poses another challenge of class imbalance.

4.2 Baselines

We compare our approach with several state-of-the-art video domain adaptation methods, image domain adaptation approaches, single-domain action recognition models, and a basic ResNet-101 classification model pre-trained on the ImageNet dataset. Single-domain action recognition models include the 3D ConvNets (C3D) [36] and Temporal Segment Networks (TSN) [39], which are pre-trained on the source domain and tested on the target domain. Four classical image-level domain adaptation methods, *i.e.*, Domain Adversarial Neural Network (DANN) [6], Joint Adaptation Network (JAN) [21], Adaptive Batch Normalization (AdaBN) [18] and Maximum Classifier Discrepancy (MCD) [32] are adjusted to align the distributions of video features with the frame aggregation module. As for non-deep video domain adaptation, we compare the proposed HABG method with Many-to-One [44] Encoder, two variants of Action Modeling on Latent Subspace (AMLS) [11], *i.e.*, the Subspace Alignment (AMLS-SA) and Geodesic Flow Kernel (AMLS-GFK). For deep video domain adaptation methods, we adopt the Deep Adversarial Action Adaptation (DAAA) [11], Temporal Adversarial Adaptation Network (TA²N) [2], Temporal Attentive Adversarial Adaptation Network (TA³N) [2] and Temporal Co-attention Network (TCoN) [29] for comparison.

4.3 Implementation Details

Our source code is based on PyTorch [30], which is available in a Github repository¹ for reference. All experiments are conducted on two servers with two GeForce GTX 2080 Ti GPUs.

4.3.1 Video Pre-processing. Following the standard protocol used in [2], we sample a fixed-number K of frames with an equal spacing from each video for training, and encode each frame with the Resnet-101 [10] pre-trained on ImageNet into a 2048-D vector, *i.e.*, $D = 2048$. For fair comparison, we set K to 5 in our experiments.

4.3.2 Module Architecture. The edge update networks \mathcal{F}_{fe} and \mathcal{F}_{ve} project the affinity map from D and D_v dimensions to 1-dim scores, which are composed of the two convolutional layers, batch normalization, LeakyReLU and edge dropout. The node update networks \mathcal{F}_{fv} and \mathcal{F}_{vn} map the $2D$ -dim and $2D_v$ -dim concatenation of node features and the neighbors' features to the D_v -dim and D_n -dim vectors, respectively. \mathcal{F}_{fv} and \mathcal{F}_{vn} include two convolutional layers, batch normalization, LeakyReLU and node dropout.

4.3.3 Parameter Settings. The hidden size, the feature dimension of frame nodes (*i.e.* D_v) and the feature dimension of video nodes (*i.e.* D_n) are fixed to 512. The total number of training epochs M is 60 for

¹https://github.com/Luoyadan/MM2020_ABG

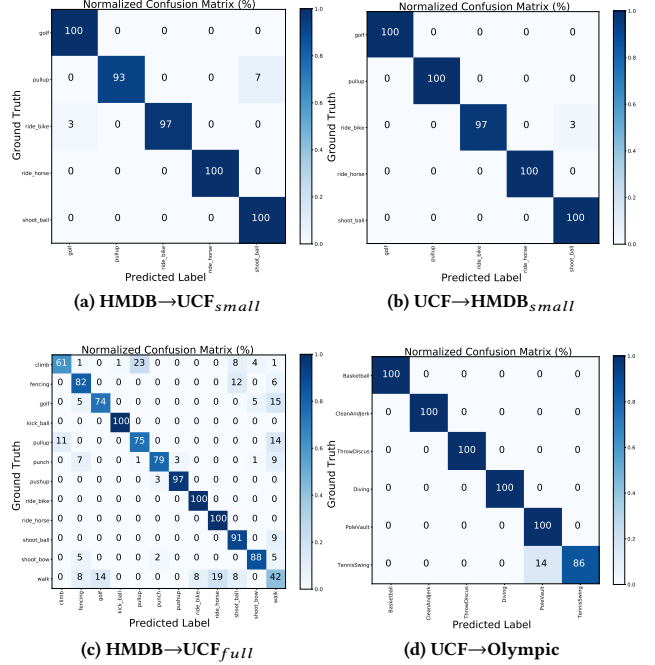


Figure 3: The confusion matrices of the proposed ABG method performed on three benchmark datasets.

Kinetics-Gameplay dataset, and 30 for the rest of datasets. The batch size B_s , B_t for the source data and target data are set to 128. The stochastic gradient optimizer (SGD) is used as the optimizer with a momentum of 0.9 and weight decay of 1×10^{-4} . The learning rate μ is initiated as 4×10^{-2} then decayed as the number of epoch increases, which follows the rule used in [2, 6]. The loss coefficients α and λ are empirically fixed at 0.1 and 1 for semi-supervised experiments. The dropout rate is set to 0.2.

4.4 Comparisons with State-of-The-Art

Under the unsupervised domain adaptation protocol, we compare the proposed ABG method with multiple baseline approaches on UCF-HMDB_{small}, UCF-Olympic and UCF-HMDB_{full} datasets. With different backbone networks, the comparison results achieved from the relatively small datasets are reported in Table 2. Table 3 presents the results on the full UCF-HMDB dataset using various frame aggregation strategies. It is observed that the proposed ABG framework is superior to all the compared image- and video-level domain adaptation methods in most cases, especially achieving a significant performance boost on the large-scale testbed. Notably, **Source Only** indicates the backbone model pretrained on the source domain and tested on the target domain. **Target Only**

Table 2: Recognition accuracies (%) on the UCF-HMDB_{small} and UCF-Olympic datasets. U: UCF, H: HMDB, O: Olympic.

Method	Backbone	U→H _{small}	H→U _{small}	U→O	O→U
Source Only	TSN	-	82.10	80.00	76.67
	C3D	-	-	82.13	83.16
Many-to-One [44]	Action Bank	82.00	82.00	87.00	75.00
AMLS-SA [11]	C3D	90.25	94.40	83.92	86.07
AMLS-GFK [11]	C3D	89.53	95.36	84.65	86.44
DAAA [11]	TSN	-	88.36	88.37	86.25
DAAA [11]	C3D	-	-	91.60	89.96
TCoN [29]	TSN	-	93.01	93.91	91.65
TA ³ N [2]	ResNet-101	99.33	99.47	98.15	92.92
ABG-AvgPool	ResNet-101	99.33	98.41	98.15	92.50

Table 3: Recognition accuracies (%) of the domain adaptation methods and the proposed ABG model with respect to various frame aggregation strategies on the full UCF-HMDB dataset.

Method	UCF→HMDB				HMDB→UCF			
	AvgPool	LSTM	GRU	TRN	AvgPool	LSTM	GRU	TRN
Source Only	70.28	69.17	70.83	71.67	74.96	70.05	76.36	73.91
DANN [6]	71.11	70.00	70.83	75.28	75.13	75.83	75.13	76.36
JAN [21]	71.39	70.56	72.50	74.72	77.58	77.58	77.75	79.36
AdaBN [18]	75.56	74.17	74.72	72.22	76.36	77.41	74.96	77.41
MCD [32]	71.67	70.00	74.44	73.89	76.18	68.30	78.81	79.34
TA ² N [2]	71.11	70.00	70.83	77.22	76.36	70.75	76.89	80.56
TA ³ N [2]	71.94	70.00	69.72	78.33	76.36	70.75	77.23	81.79
ABG	79.17	75.56	75.56	76.67	85.11	84.24	83.36	81.79
Target Only	80.56	-	-	82.78	92.12	-	-	94.92

denotes the backbone model trained and tested on the target domain. From Table 2, it is demonstrated that the deep video DA methods (line 6-10) generally outperforms the non-deep video DA approaches (line 3-5) and the classification models without DA (line 1-2). Among the deep TCoN and TA³N leverage the attention mechanism and then suppress the variance caused by the outlier frames, improving the recognition accuracy by up to 6.3% and 11.1% over DAAA on the UCF-Olympic dataset. With the same backbone of TA³N, our ABG model performs comparably without relying on the frame attention or complex frame aggregation strategies. This phenomenon is also observed in the large UCF-HMDB_{full} dataset, in which the proposed ABG with the average pooling boosts the performance by up to 10.1% and 11.5% over the state-of-the-art TA³N on the UCF→HMDB and HMDB→UCF tasks, respectively. As shown in Table 3, average pooling (AvgPool) and LSTM suits the proposed model better among other frame aggregation functions. We infer the reasons behind is the frame bipartite graph has already fused similar frames regardless the order, which weakens the power of multi-scaled TRN aggregation. Notably, it is observed that AdaBN surpasses the most of image domain adaptation methods. As it separates the batch normalization layer for source and target data, AdaBN minimizes the risk of being overfitting to the source domain, which provides a strong support to our statement discussed in Section 1. To further investigate the detailed performance of the proposed ABG with respect to specific classes, four confusion matrices are provided in Figure 3.

Table 4: Experimental results under the semi-supervised setting on the Kinetics-Gameplay dataset.

Method	Kinetics→Gameplay				Gameplay→Kinetics			
	30%	50%	70%	90%	30%	50%	70%	90%
Source Only	16.29	16.29	16.29	16.29	14.82	14.82	14.82	14.82
DANN [6]	49.67	56.74	60.48	65.02	33.24	40.05	40.44	43.38
JAN [21]	47.40	53.94	60.35	61.28	32.69	22.95	41.31	32.75
AdaBN [18]	55.54	59.95	64.62	67.56	44.82	47.67	47.73	48.00
MCD [32]	47.53	52.60	57.68	59.95	36.29	40.08	41.13	42.05
TA ² N [2]	57.14	60.08	64.09	65.02	42.39	44.82	44.39	45.66
TA ³ N [2]	56.61	62.35	63.02	63.95	43.25	44.27	44.02	42.05
Semi-ABG	57.28	64.35	65.42	68.36	59.80	62.19	62.46	63.67
Semi-HABG	61.15	65.29	67.29	70.36	60.39	62.54	63.36	63.98
Target Only	54.21	58.88	61.55	66.62	39.96	42.54	44.58	44.36

4.5 Semi-supervised Learning

To study the robustness of the proposed algorithm, we extend the unsupervised domain adaptation to a semi-supervised setting, where a part of target labels are available for training. Extensive experiments are conducted on the most challenging “Synthetic-to-Real” testbed, *i.e.*, the **Kinetics-Gameplay** dataset, on which the results with varying ratios of target labels are reported in Table 4. The seen ratio of target labels ranges from 0.3 to 0.9. Similarly, **Source Only** / **Target only** represents the backbone model trained with source / target data only. All image-level domain adaptation methods (line 2-5), basic classification model (line 1,10) and our models (line 8-9) utilize **AvgPool** as the frame aggregation function. TA²N and TA³N use the TRN aggregator, since TRN is the major part of their works. It can be seen that the overall performance is lower on the **Gameplay→Kinetics** compared to **Kinetics→Gameplay**, due to the insufficient samples in the source domain. The proposed **Semi-ABG** and its hierarchical variant **Semi-HABG** achieve higher recognition accuracy on both two transfer tasks, since the integrated graphs help to propagate the label information and take a full advantage of the supervision. The respective recognition accuracies of the proposed HABG on two transfer tasks are improved by up to 8.0% and 39.6% over the state-of-the-art TA³N with only 30% of target labels available.

4.6 Ablation Study

To investigate the validity of the derived modules and objective functions, we compare the four variants of ABG model on the full UCF-HMDB dataset. The comparison results are summarized in Table 5. Removing the bipartite graphs, the **ABG w/o Graph** suffers a drop dramatically compared with the full model. The **ABG w/o \mathcal{L}_d** is the variant without the conditional adversarial learning, decreasing the recognition accuracy by 8.4% and 2.95% on average for the UCF→HMDB and HMDB→UCF tasks, respectively. The **ABG w/o \mathcal{L}_y^t** refers to the variant without the entropy loss for target data, which triggers a slight decrease on the model performance. **HABG** is the hierarchical variant of the plain ABG model, performing better on the challenging UCF→HMDB transfer task, which is consistent with the findings in semi-supervised experiments. The **ABG** model is more versatile and suitable for small datasets and easier transfer tasks such as HMDB→UCF.

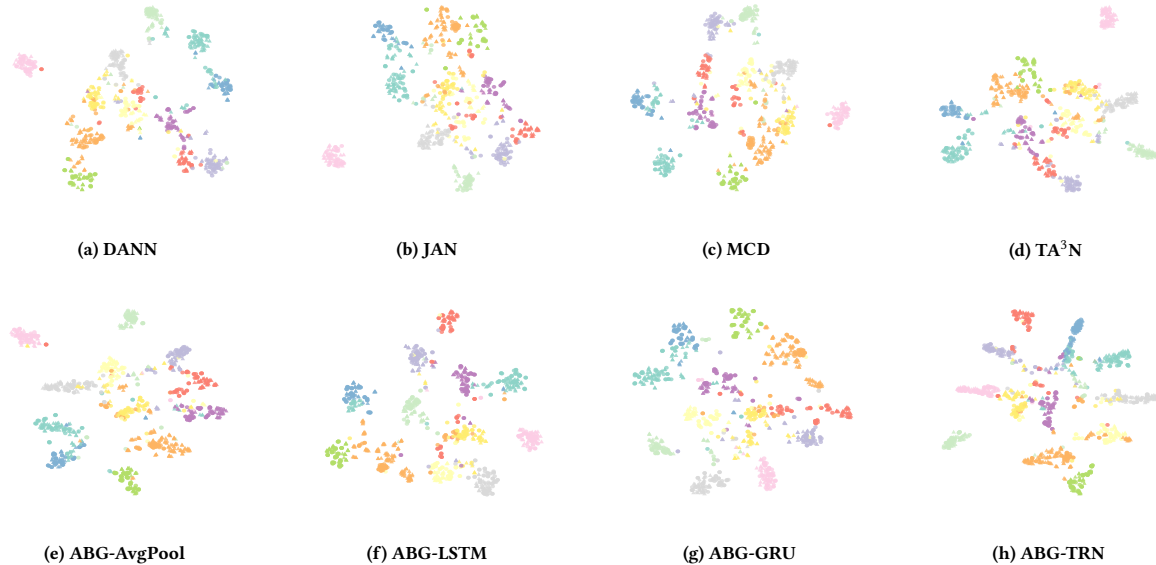


Figure 4: The t-SNE visualization of the learned source and target video representations on the HMDB→UCF task.

Table 5: The ablation performance of the proposed ABG and HABG models on the full UCF-HMDB dataset.

Method	UCF→HMDB _{full}		HMDB→UCF _{full}	
	AvgPool	TRN	AvgPool	TRN
ABG w/o Graph	71.39	73.89	74.96	74.61
ABG w/o \mathcal{L}_d	72.78	70.00	82.14	79.86
ABG w/o \mathcal{L}_y^t	78.33	75.83	82.67	81.79
HABG	80.00	76.94	82.49	80.21
ABG	79.17	76.67	85.11	81.79

4.7 Parameter Sensitivity

To study the effect of the loss coefficients, we conduct the experiments on the UCF-HMDB_{full} dataset with the varying values of β and γ . The β and γ are utilized to reconcile the adversarial loss and the entropy loss, respectively. We compare the proposed ABG model and its variant HABG integrated with the identical AvgPool frame aggregation function. As plotted in Figure 5, the average accuracies for both ABG and HABG models become quite stable when reaching sufficiently large loss coefficients. This indicates that our framework is robust with respect to loss coefficients.

4.8 Visualization

To shed a qualitative light on evaluating the proposed model with various aggregation functions, we conduct the experiments on the HMDB→UCF task, and visualize the features with t-SNE in Figure 4. The features are extracted from the last layer of ABG and the baseline models, including DANN, JAN, MCD and TA³N. Different colors indicate different classes. Circles represent the source videos and triangles represent the target videos. It is clearly shown that the features from ABG achieve the tighter clusters compared to the baselines.

5 CONCLUSION

In this work, we propose a bipartite graph learning framework for unsupervised and semi-supervised video domain adaptation tasks. Different the existing approaches which learn domain-invariant features, we construct a domain-agnostic classifier by leveraging the

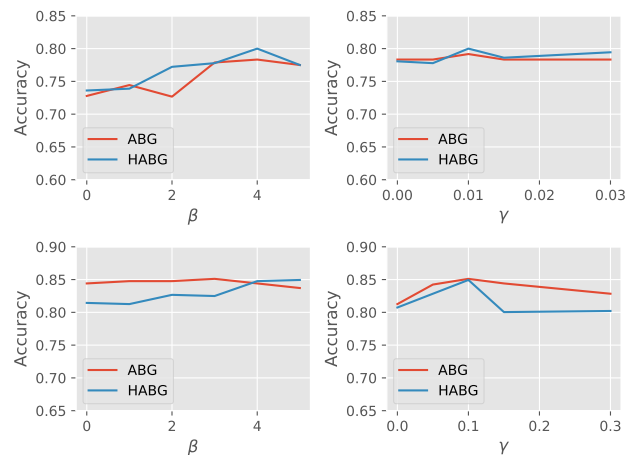


Figure 5: Performance comparisons of the proposed ABG and HABG with respect to the varying loss coefficients on the UCF→HMDB (shown in the upper row) and HMDB→UCF (shown in the bottom row) tasks.

bipartite graphs to combine the similar source and target features at the training and test time, which helps with reducing the exposure bias. Experiments evidence effectiveness of our proposed approach over the state-of-the-art methods, improving their performance by up to 39.6% in a semi-supervised setting.

ACKNOWLEDGMENTS

This work was partially supported by ARC DP 190102353.

REFERENCES

- [1] Mahsa Baktashmotlagh, Mehrtaash Tafazzoli Harandi, Brian C. Lovell, and Mathieu Salzmann. 2014. Domain Adaptation on the Statistical Manifold. In *Proc. IEEE Conference on Computer Vision and Pattern Recognition (CVPR)*. 2481–2488.
- [2] Min-Hung Chen, Zsolt Kira, Ghassem AlRegib, Jaekwon Woo, Ruxin Chen, and Jian Zheng. 2019. Temporal Attentive Alignment for Large-Scale Video Domain Adaptation. *CoRR* abs/1907.12743 (2019). arXiv:1907.12743
- [3] Zhi Chen, Jingjing Li, Yadan Luo, Zi Huang, and Yangyang Yangyang. 2020. CANZSL: Cycle-Consistent Adversarial Networks for Zero-Shot Learning from

- Natural Language. In *IEEE Winter Conference on Applications of Computer Vision, WACV*. 863–872.
- [4] Jeff Donahue, Lisa Anne Hendricks, Marcus Rohrbach, Subhashini Venugopalan, Sergio Guadarrama, Kate Saenko, and Trevor Darrell. 2017. Long-Term Recurrent Convolutional Networks for Visual Recognition and Description. *IEEE Transactions on Pattern Analysis and Machine Intelligence* 39, 4 (2017), 677–691.
 - [5] Xuguang Duan, Wen-bing Huang, Chuang Gan, Jingdong Wang, Wenwu Zhu, and Junzhou Huang. 2018. Weakly Supervised Dense Event Captioning in Videos. In *Proc. Advances in Neural Information Processing Systems (NeurIPS)*. 3063–3073.
 - [6] Yaroslav Ganin, Evgeniya Ustinova, Hana Ajakan, Pascal Germain, Hugo Larochelle, François Laviolette, Mario Marchand, and Victor S. Lempitsky. 2016. Domain-Adversarial Training of Neural Networks. *Journal of Machine Learning Research* 17 (2016), 59:1–59:35.
 - [7] Boqing Gong, Kristen Grauman, and Fei Sha. 2013. Connecting the Dots with Landmarks: Discriminatively Learning Domain-Invariant Features for Unsupervised Domain Adaptation. In *Proc. Int. Conference on Machine Learning (ICML)*. 222–230.
 - [8] Arthur Gretton, Karsten M. Borgwardt, Malte J. Rasch, Bernhard Schölkopf, and Alexander J. Smola. 2012. A Kernel Two-Sample Test. *Journal of Machine Learning Research* 13 (2012), 723–773.
 - [9] William L. Hamilton, Zhitaoying, and Jure Leskovec. 2017. Inductive Representation Learning on Large Graphs. In *Proc. Advances in Neural Information Processing Systems (NeurIPS)*. 1024–1034.
 - [10] Kaiming He, Xiangyu Zhang, Shaoqing Ren, and Jian Sun. 2016. Deep Residual Learning for Image Recognition. In *Proc. IEEE Conference on Computer Vision and Pattern Recognition (CVPR)*. 770–778.
 - [11] Arshad Jamal, Vinay P. Nambodiri, Dipti Deodhare, and K. S. Venkatesh. 2018. Deep Domain Adaptation in Action Space. In *Proc. British Machine Vision Conference (BMVC)*. 264.
 - [12] Andrej Karpathy, George Toderici, Sanketh Shetty, Thomas Leung, Rahul Sukthankar, and Fei-Fei Li. 2014. Large-Scale Video Classification with Convolutional Neural Networks. In *Proc. IEEE Conference on Computer Vision and Pattern Recognition (CVPR)*. 1725–1732.
 - [13] Will Kay, João Carreira, Karen Simonyan, Brian Zhang, Chloe Hillier, Sudheendra Vijayanarasimhan, Fabio Viola, Tim Green, Trevor Back, Paul Natsev, Mustafa Suleyman, and Andrew Zisserman. 2017. The Kinetics Human Action Video Dataset. *CoRR abs/1705.06950* (2017). arXiv:1705.06950
 - [14] Thomas N. Kipf and Max Welling. 2017. Semi-Supervised Classification with Graph Convolutional Networks. In *Proc. Int. Conference on Learning Representations (ICLR)*.
 - [15] Ranjay Krishna, Kenji Hata, Frederic Ren, Li Fei-Fei, and Juan Carlos Niebles. 2017. Dense-Captioning Events in Videos. In *Proc. Int. Conference on Computer Vision (ICCV)*. 706–715.
 - [16] Hildegard Kuehne, Hueihuan Jhuang, Estíbaliz Garrote, Tomaso A. Poggio, and Thomas Serre. 2011. HMDB: A large video database for human motion recognition. In *Proc. Int. Conference on Computer Vision (ICCV)*. 2556–2563.
 - [17] Chang-Uk Kwak, Minho Han, Sun-Joong Kim, and Gyeong-June Hahm. 2018. Interactive Story Maker: Tagged Video Retrieval System for Video Re-creation Service. In *Proc. ACM International Conference on Multimedia (MM)*. 1270–1271.
 - [18] Yanghao Li, Naiyan Wang, Jianping Shi, Xiaodi Hou, and Jiaying Liu. 2018. Adaptive Batch Normalization for practical domain adaptation. *Pattern Recognition* 80 (2018), 109–117.
 - [19] Jun Liu, Gang Wang, Ping Hu, Ling-Yu Duan, and Alex C. Kot. 2017. Global Context-Aware Attention LSTM Networks for 3D Action Recognition. In *Proc. IEEE Conference on Computer Vision and Pattern Recognition (CVPR)*. 3671–3680.
 - [20] Mingsheng Long, Zhangjie Cao, Jianmin Wang, and Michael I. Jordan. 2018. Conditional Adversarial Domain Adaptation. In *Proc. Advances in Neural Information Processing Systems (NeurIPS)*. 1647–1657.
 - [21] Mingsheng Long, Han Zhu, Jianmin Wang, and Michael I. Jordan. 2017. Deep Transfer Learning with Joint Adaptation Networks. In *Proc. Int. Conference on Machine Learning (ICML)*. 2208–2217.
 - [22] Yadan Luo, Zi Huang, Zheng Zhang, Ziwei Wang, Mahsa Baktashmotlagh, and Yang Yang. 2020. Learning from the Past: Continual Meta-Learning with Bayesian Graph Neural Networks. In *Proc. AAAI Conference on Artificial Intelligence*. 5021–5028.
 - [23] Yadan Luo, Zi Huang, Zheng Zhang, Ziwei Wang, Jingjing Li, and Yang Yang. 2019. Curiosity-driven Reinforcement Learning for Diverse Visual Paragraph Generation. In *Proc. ACM International Conference on Multimedia (MM)*. 2341–2350.
 - [24] Yadan Luo, Zijian Wang, Zi Huang, and Mahsa Baktashmotlagh. 2020. Progressive Graph Learning for Open-Set Domain Adaptation. In *Proc. International Conference on Machine Learning (ICML)*.
 - [25] Chih-Yao Ma, Asim Kadav, Iain Melvin, Zsolt Kira, Ghassan AlRegib, and Hans Peter Graf. 2018. Attend and Interact: Higher-Order Object Interactions for Video Understanding. In *Proc. IEEE Conference on Computer Vision and Pattern Recognition (CVPR)*. 6790–6800.
 - [26] Xinhong Ma, Tianzhu Zhang, and Changsheng Xu. 2019. GCAN: Graph Convolutional Adversarial Network for Unsupervised Domain Adaptation. In *Proc. IEEE Conference on Computer Vision and Pattern Recognition (CVPR)*. 8266–8276.
 - [27] Juan Carlos Niebles, Chih-Wei Chen, and Fei-Fei Li. 2010. Modeling Temporal Structure of Decomposable Motion Segments for Activity Classification. In *Proc. European Conference on Computer Vision (ECCV)*. 392–405.
 - [28] Deqiang Ouyang, Jie Shao, Yonghui Zhang, Yang Yang, and Heng Tao Shen. 2018. Video-based Person Re-identification via Self-Paced Learning and Deep Reinforcement Learning Framework. In *Proc. ACM International Conference on Multimedia (MM)*. 1562–1570.
 - [29] Boxiao Pan, Zhangjie Cao, Ehsan Adeli, and Juan Carlos Niebles. 2019. Adversarial Cross-Domain Action Recognition with Co-Attention. *CoRR abs/1912.10405* (2019). arXiv:1912.10405
 - [30] Adam Paszke, Sam Gross, Francisco Massa, Adam Lerer, James Bradbury, Gregory Chanan, Trevor Killeen, Zeming Lin, Natalia Gimelshein, et al. 2019. PyTorch: An Imperative Style, High-Performance Deep Learning Library. In *Proc. Advances in Neural Information Processing Systems (NeurIPS)*. 8024–8035.
 - [31] Hossein Rahmani and Mohammed Bennamoun. 2017. Learning Action Recognition Model from Depth and Skeleton Videos. In *Proc. Int. Conference on Computer Vision (ICCV)*. 5833–5842.
 - [32] Kuniaki Saito, Kohei Watanabe, Yoshitaka Ushiku, and Tatsuya Harada. 2018. Maximum Classifier Discrepancy for Unsupervised Domain Adaptation. In *Proc. IEEE Conference on Computer Vision and Pattern Recognition (CVPR)*. 3723–3732.
 - [33] Karen Simonyan and Andrew Zisserman. 2014. Two-Stream Convolutional Networks for Action Recognition in Videos. In *Proc. Advances in Neural Information Processing Systems (NeurIPS)*. 568–576.
 - [34] Khuram Soomro, Amir Roshan Zamir, and Mubarak Shah. 2012. UCF101: A Dataset of 101 Human Actions Classes From Videos in The Wild. *CoRR abs/1212.0402* (2012). arXiv:1212.0402
 - [35] Jun Tang, Haiqun Jin, Shoubiao Tan, and Dong Liang. 2016. Cross-domain action recognition via collective matrix factorization with graph Laplacian regularization. *Image and Vision Computing* 55 (2016), 119–126.
 - [36] Du Tran, Lubomir D. Bourdev, Rob Fergus, Lorenzo Torresani, and Manohar Paluri. 2015. Learning Spatiotemporal Features with 3D Convolutional Networks. In *Proc. Int. Conference on Computer Vision (ICCV)*. 4489–4497.
 - [37] Petar Velickovic, Guillem Cucurull, Arantxa Casanova, Adriana Romero, Pietro Liò, and Yoshua Bengio. 2018. Graph Attention Networks. In *Proc. Int. Conference on Learning Representations (ICLR)*.
 - [38] Junbo Wang, Wei Wang, Yan Huang, Liang Wang, and Tieniu Tan. 2018. Hierarchical Memory Modelling for Video Captioning. In *Proc. ACM International Conference on Multimedia (MM)*. 63–71.
 - [39] Limin Wang, Yuanjun Xiong, Zhe Wang, Yu Qiao, Dahua Lin, Xiaoou Tang, and Luc Van Gool. 2016. Temporal Segment Networks: Towards Good Practices for Deep Action Recognition. In *Proc. European Conference on Computer Vision (ECCV)*. 20–36.
 - [40] Ziwei Wang, Zi Huang, and Yadan Luo. 2020. Human Consensus-Oriented Image Captioning. In *Proc. International Joint Conference on Artificial Intelligence, IJCAI*. 659–665.
 - [41] Zijian Wang, Zheng Zhang, Yadan Luo, and Zi Huang. 2019. Deep Collaborative Discrete Hashing with Semantic-Invariant Structure. In *Proc. International ACM SIGIR Conference on Research and Development in Information Retrieval, SIGIR*. 905A–908.
 - [42] Yinwei Wei, Zhiyong Cheng, Xuzheng Yu, Zhou Zhao, Lei Zhu, and Liqiang Nie. 2019. Personalized Hashtag Recommendation for Micro-videos. In *Proc. ACM International Conference on Multimedia (MM)*. 1446–1454.
 - [43] Yinwei Wei, Xiang Wang, Liqiang Nie, Xiangnan He, Richang Hong, and Tat-Seng Chua. 2019. MMGCN: Multi-modal Graph Convolution Network for Personalized Recommendation of Micro-video. In *Proc. ACM International Conference on Multimedia (MM)*. 1437–1445.
 - [44] Tiantian Xu, Fan Zhu, Edward K. Wong, and Yi Fang. 2016. Dual many-to-one-encoder-based transfer learning for cross-dataset human action recognition. *Image and Vision Computing* 55 (2016), 127–137.
 - [45] An Yan, Yali Wang, Zhifeng Li, and Yu Qiao. 2019. PA3D: Pose-Action 3D Machine for Video Recognition. In *Proc. IEEE Conference on Computer Vision and Pattern Recognition (CVPR)*. 7922–7931.
 - [46] Hongliang Yan, Yukang Ding, Peihua Li, Qilong Wang, Yong Xu, and Wangmeng Zuo. 2017. Mind the Class Weight Bias: Weighted Maximum Mean Discrepancy for Unsupervised Domain Adaptation. In *Proc. IEEE Conference on Computer Vision and Pattern Recognition (CVPR)*. 945–954.
 - [47] Ziwei Yang, Yahong Han, and Zheng Wang. 2017. Catching the Temporal Regions-of-Interest for Video Captioning. In *Proc. ACM International Conference on Multimedia (MM)*. 146–153.
 - [48] Han Zhao, Remi Tachet des Combes, Kun Zhang, and Geoffrey J. Gordon. 2019. On Learning Invariant Representations for Domain Adaptation. In *Proc. Int. Conference on Machine Learning (ICML)*. 7523–7532.
 - [49] Bolei Zhou, Alex Andonian, Aude Oliva, and Antonio Torralba. 2018. Temporal Relational Reasoning in Videos. In *Proc. European Conference on Computer Vision (ECCV)*. 831–846.